International Journal of Pressure Vessels and Piping 132-133 (2015) 65–71

Contents lists available at ScienceDirect

International Journal of Pressure Vessels and Piping

journal homepage: www.elsevier.com/locate/ijpvp

Electromagnetic evaluation of the microstructure of Grade 91 tubes/pipes

Jun Liu [a, *], John Wilson [b], Martin Strangwood [a], Claire L. Davis [a, 1], Anthony Peyton [b], Jonathan Parker [c]

[a] School of Metallurgy and Materials, University of Birmingham, Edgbaston, Birmingham B15 2TT, UK
[b] School of Electrical and Electronic Engineering, The University of Manchester, Manchester M13 9PL, UK
[c] Electrical Power Research Institute, 1300 West W.T. Harris Boulevard, Charlotte NC 28262, USA

ARTICLE INFO

Article history:
Received 11 June 2014
Received in revised form
27 March 2015
Accepted 12 May 2015
Available online 3 June 2015

Keywords:
Grade 91 steel
EM sensor
Relative permeability
BH loop
Tube

ABSTRACT

This paper assesses the feasibility of transferring a laboratory-based electromagnetic (EM) sensor technique, which has already proved sensitive to significant (e.g. phase balance) or subtle (e.g. number density of fine precipitates) microstructural changes in steel, to non-destructive evaluation of the microstructure of power generation components such as tubes/pipes. It has been found that Grade 91 steels, in different conditions representative of service entry, thermally aged or ex-service, can be distinguished using laboratory-based measurement systems on small machined cylindrical samples as well as by an industry deployment EM sensor system on full-diameter tube samples. The measurements for the tube samples follow the same trend as the machined cylindrical samples. The results indicate an industrial deployable sensor system can be used for sorting service-exposed or mis-heat-treated/mis-manufactured Grade 91 steel tubes/pipes from the correctly heat treated service-entry ones.

1. Introduction

Grade 91 steels are widely used in the power generation industry for high-temperature components such as boiler tubes and steamline pipes. They are usually heat treated or supplied in the as normalized and tempered condition before entering service [1]. However, there is evidence that mis-manufactured, or mis-heat-treated, materials/components have been supplied [2]. Importantly, traditional methods for quality checking have not always identified the presence of the mal-heat treatment [3]. Using a component with an incorrect microstructure in service has resulted in product failure at times below that expected by that of Design Codes [4]. To avoid mis-heat-treated material from entering service a fast, accurate and non-destructive sorting tool is needed. Commercial sorting tools such as the X-Ray fluorescence analyzer, which can sort steel grades by analyzing the alloy element contents, are not sensitive to microstructure and hence not able to distinguish between steels of the same grade but different microstructures due to different heat treatment conditions or service history. The conventional inspection techniques for microstructure assessment currently used by the power generation industries, such as examination of surface replicas or hardness measurements are only suitable for limited spot checks [3]. Moreover hardness measurement lacks specificity to fine microstructural detail, and similar information can result from steels with a surface decarburisation layer compared to mis-heat-treated steels. Thus, a non-destructive technique, to complement hardness testing, for the assessment of the microstructure in Grade 91 steels would be of significant benefit.

Magnetic hysteresis loop (or BH loop) and Magnetic Barkhausen Emission (MBE) techniques have been used to evaluate microstructural changes in Grade 91 steels during creep tests under 125 MPa stress at 600 °C [5,6] or tempering at different temperatures (ranging from 650 °C to 950 °C) [7]. Changes in the magnetic properties such as coercivity (H_c) and remanence (B_r) or the MBE parameters such as the peak height/position of the root mean square (RMS) of voltage profiles were correlated to microstructural

* Corresponding author. Present address: Warwick Manufacturing Group, University of Warwick, Coventry CV4 7AL, UK. The underlying data behind this article may be accessed through the corresponding author.
E-mail addresses: sam.j.liu@gmail.com, j.liu.2@warwick.ac.uk (J. Liu), john.wilson@manchester.ac.uk (J. Wilson), m.strangwood@bham.ac.uk (M. Strangwood), Claire.Davis@warwick.ac.uk (C.L. Davis), a.peyton@manchester.ac.uk (A. Peyton), jparker@epri.com (J. Parker).
[1] Present address: Warwick Manufacturing Group, University of Warwick, Coventry CV4 7AL, UK.

http://dx.doi.org/10.1016/j.ijpvp.2015.05.009

Nomenclature

μ_r	relative permeability
ω	angular frequency
B	magnetic induction
B_r	remanence
H	magnetic field strength
H_c^*	coercive force for the non-saturated major loops for the tubes
H_c	coercivity
M	mutual inductance
M_0	inductance at low frequencies
Z	trans-impedance
EM	Electromagnetic
LMP	Larson–Miller parameter
MBE	Magnetic Barkhausen Emission
PIRMP	Peak Interval of Reversible Magnetic Permeability

changes (e.g. precipitation of large carbides or Laves phase [5,6]), mechanical hardness [7], or used to indicate different creep stages [5]. Moorthy reported double peaks in the MBE profiles for a P9 and a T22 steel after tempering for different times and correlated them generally to the domain walls overcoming pinning from precipitates or grain boundaries respectively [8]; however, the role of the precipitate location e.g. on the martensitic lath boundaries (expected to be minor) or within the laths (important role) was not considered. Bong et al. [9] reported evaluating remnant life of Grade 91 steels by looking at the relationship between a parameter called Peak Interval of Reversible Magnetic Permeability (PIRMP ≈ twice the coercivity force) measured using a laboratory-based EM sensor system and the Larson–Miller parameter (LMP). It was reported that the PIRMP data were practically insensitive to the Larson–Miller parameter after a LMP of 21965 (i.e. equivalent to a thermal exposure at 610 °C for 75,000 h or about 8.5 years, which would still be in the early stage of the expected service life for a T91 steel tube) and whilst the mechanical properties, such as yield stress or tensile strength, are much more sensitive than the PIRMP to the LMP.

Multi-frequency EM sensors have proved sensitive to changes in ferrite (α)/austenite (γ), shown using model alloys, in-situ analysis and FE based modeling software [10,11]. Prototype EM sensors are being used for in-situ monitoring of the $\gamma \rightarrow \alpha$ transformation during steel processing [12]. EM sensors have also been used to detect decarburisation, shown with high carbon steels for on-line and off-line monitoring [13,14]. The theory as to how the relative permeability and resistivity of a sample affect the multi-frequency EM response, for any sensor geometry, is presented elsewhere [15]. It has been shown that the multi-frequency EM sensors are able to detect the initial relative permeability and resistivity changes, resulting from microstructural changes in P9 and T22 power plant steels during service at high temperatures [16]. The developed laboratory-based EM sensor is also capable of differentiating P91 steels with different N:Al ratios in the short term tempered or long term aged condition, based on the principle that the N:Al ratio significantly affects the number density of intra-lath MX carbonitride precipitates [17]. These precipitates determine the mean free path to magnetic domain wall motion and hence the initial relative permeability of the steels and the EM signals.

Whilst a variety of related EM systems for microstructural changes have been developed for laboratory-based assessment there are no reports of industrial deployable sensors which have been successful in sorting mis-heat treated materials. This paper assesses the feasibility of transferring the present laboratory-based EM sensor technique that has already proved sensitive to microstructural changes, to non-destructive evaluation of the microstructure of power generation components such as steel tubes/pipes. Potential applications include sorting materials e.g. the mis-heat-treated or mis-manufactured materials from normal service-entry ones, amongst others, such as microstructural changes during service.

2. Materials and experimental details

T91 steel tubes (53 mm outer diameter, 13.5 mm wall thickness and >900 mm length) were supplied by the Electrical Power Research Institute (EPRI) as normalized at 1060 °C for 20 min and tempered at 780 °C for 1 h. The chemical composition of the steel is given in Table 1. Cylindrical samples (4.95 mm diameter and 100 mm length) were machined from the tube for EM sensor measurements using a laboratory-based cylindrical sensor and a laboratory-based BH loop measurement system. Selected cylindrical samples have been heat treated to different conditions in laboratory furnaces to simulate the microstructures expected of prolonged thermal exposure by accelerated tempering at 780 °C for 100 h or mis-heat treatments/mis-manufacturing. The accelerated tempering condition was chosen because it generated significant microstructural degradation and was also achievable for large demonstration tube samples. The mis-heat-treatment was simulated by the following procedure [18] in order to generate a partially ferritic structure rather than a fully martensitic one on air cooling:

1) heating up to 950 °C and dwelling for 30 min;
2) programmed furnace cooling by 100 °C/h down to 760 °C;
3) dwelling for 3 h;
4) cooling in still air.

These heat treatments were carried out on two lengths (250 mm length) of full diameter tube samples, for demonstration trials, in industrial furnaces. T91 tubes of approximately 44.5 mm outer diameter, 6.3 mm wall thickness and <70 mm length that had been taken from service as an antler tube on a superheater outlet header at 585 °C under 16.5 MPa pressure (designed) for about 50,000 h were supplied. The specific chemical composition of the steel is not presently available but the composition did comply with the applicable specification. Cylindrical samples (4.95 mm diameter and 50 mm length) were machined from the tube for EM measurements.

Metallographic samples were polished to a 0.25 μm diamond paste finish and etched in Kallings reagent. A Field Emission Gun Scanning Electron Microscope (FEG–SEM) and an EDS system were used to obtain SEM micrographs and analyze alloy contents at selected points/areas. Additional metallographic samples were polished to a 1 μm diamond paste finish followed by several etching–polishing cycles and a final polishing with OPS (oxide polishing suspension) for 10 min for electron backscattering diffraction (EBSD) analysis using an EBSD in a FEG–SEM. Lath boundaries and grain boundaries in SEM micrographs were reconstructed as trace features and objects respectively using Image–Pro Plus. Average distances between two neighbouring trace features were taken as the lath width.

A four-point probe technique was employed to independently measure the resistivity of the steels with a direct current Cropico DO5000 micro-ohmmeter at room temperature using machined cylinder specimens of 4.95 mm diameter. The resistivity values were used as input into a Comsol model (described later) to determine the relative permeability values.

Table 1
Chemical composition (weight percent) of the as-received T91 tube materials.

C	Si	Mn	P	S	Cr	Mo	Ni	V	Nb	N	Ti
0.11	0.271	0.469	0.015	0.003	8.9	1.00	0.135	0.169	0.055	0.046	0.003

A cylindrical EM sensor consisting of one exciting coil and one sensing coil both wound around an insulating tube of 5.5 and 6.5 mm inner and outer diameters, respectively, was used to carry out the EM sensor tests on the same cylindrical specimens as for the resistivity measurements. The sensor was operated at 3 V and over a range of frequencies from 10 Hz to 1 MHz. Signals detected by the sensing coil were recorded and processed by a Solartron Analytical Model S1260 Impedance Analyzer to give the complex trans-impedance Z, from which the mutual inductance M was calculated as $M = Z/j\omega$ where ω is angular frequency and j the imaginary unit.

A schematic diagram of the system, developed to measure magnetic major and minor loops, for the machined cylindrical samples is shown in Fig. 1. A low frequency time varying signal is fed to two power amplifiers, which supply current to two excitation coils wrapped around a silicon-steel core. The cylindrical sample is fitted into a slot in the core, to maximise coupling between the core and sample. The axial applied field (H) is measured using a Quantum Well Hall sensor, developed by Professor M Missous at the University of Manchester [19]. The flux density of the induced field (B) is measured using a 20–turn encircling coil connected to an instrumentation amplifier. For the major loops, 1 Hz sinusoidal excitation is used and 9 cycles are recorded and averaged.

The test system used for the demonstration tube samples (Fig. 2) is an adaptation of the laboratory-based system shown in Fig. 1. A U–core, contoured to the profile of the tube, provides excitation. The excitation system is similar to that shown in Fig. 1; in this case the U–core is wrapped with two 160–turn excitation coils. Field strength, H, measurement is accomplished using a Quantum Well Hall sensor positioned 1.8 mm from the sample surface. Flux density, B, measurement is inferred via a 10–turn coil, encircling the leg of the excitation yoke. The signal conditioning system and signal processing techniques are similar to those detailed for the laboratory-based system described above.

3. Results and discussion

3.1. Microstructures

The as-received T91 tube (T91-AR) shows a microstructure of tempered martensite consisting of martensitic laths with many precipitates (mainly $M_{23}C_6$) on the lath boundaries, as shown in Fig. 3.

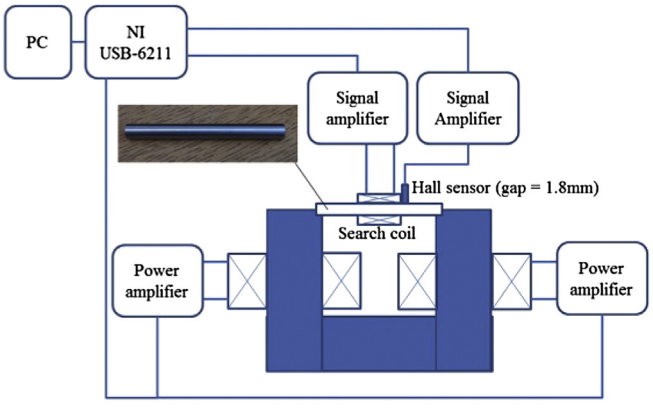

Fig. 1. A schematic of BH loop, minor loop and MBN measurement system for cylindrical machined samples.

Fig. 4 shows the distribution of the martensitic lath widths with a mode value at around 0.37 μm. The mean lath width (0.36±0.18 μm) is consistent with the reported typical lath width for service-entry Grade 91 steel (0.25–0.5 μm [20]). No precipitates can be observed within the laths, in these scanning electron micrographs, Fig. 3(b). It should be noted that precipitates within laths would typically be MX type with an average size of around 45 nm [21].

After tempering at 780 °C for 100 h, the laths and the precipitates have significantly coarsened and a number of equi-axed sub-grains have developed. A typical micrograph is shown in Fig. 5. This figure indicates that a significant degeneration of the tempered martensite (i.e. loss of martensitic lath structure as a result of the development of equi-axed sub-grains) had occurred. The degree of change in the microstructure is comparable with degeneration due to prolonged service exposure [22,23]. Most of the precipitates are still on the lath boundaries or the sub-grain boundaries and some relatively fine precipitates now resolvable within the sub-grains or laths.

The simulated mis-heat treatment successfully produced a ferritic microstructure consisting of equi-axed ferrite grains, as expected from industry experience [18]. A high number density of coarse precipitates were present on the ferrite grain boundaries and many coarse and fine precipitates were observed within the grains, as shown in Fig. 6(a). Fig. 6(b) shows the distribution of the ferrite grain sizes (equivalent circle diameter) with a range of 3.0–26.7 μm, a mode of 8.4 μm and a mean and standard deviation of 12.0±6.6 μm indicating a significant increase in effective microstructural scale compared with correctly heat treated martensite lath width.

The ex-service T91 (T91-ES) tube shows a microstructure of slightly degenerated martensite with slightly increased lath size as compared to the T91-AR sample and some equi-axed subgrains having developed, as shown in Fig. 7(a). Few precipitates within the laths or grains have been observed as shown in Fig. 7(b).

3.2. EM measurements

3.2.1. Laboratory-based cylindrical EM sensor measurements

Fig. 8 shows EM measurements of the real part of the mutual inductance as a function of frequency for the T91 samples in the

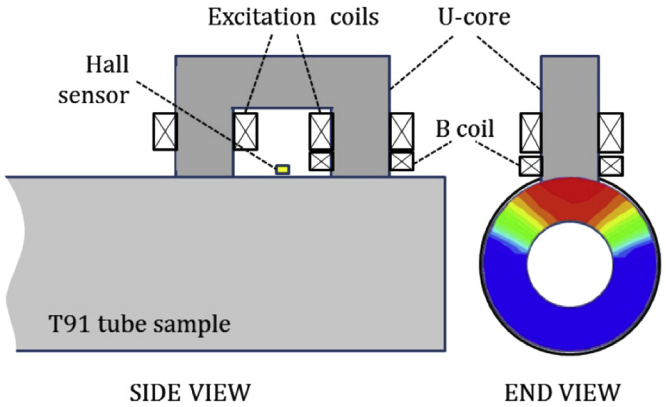

Fig. 2. BH loop measurement system for tube samples. The colors of the cross-section of the tube schematically indicate the magnetic flux density values (red denotes high values and blue low values) during a test modeled with Comsol Multiphysics. (For interpretation of the references to colour in this figure legend, the reader is referred to the web version of this article.)

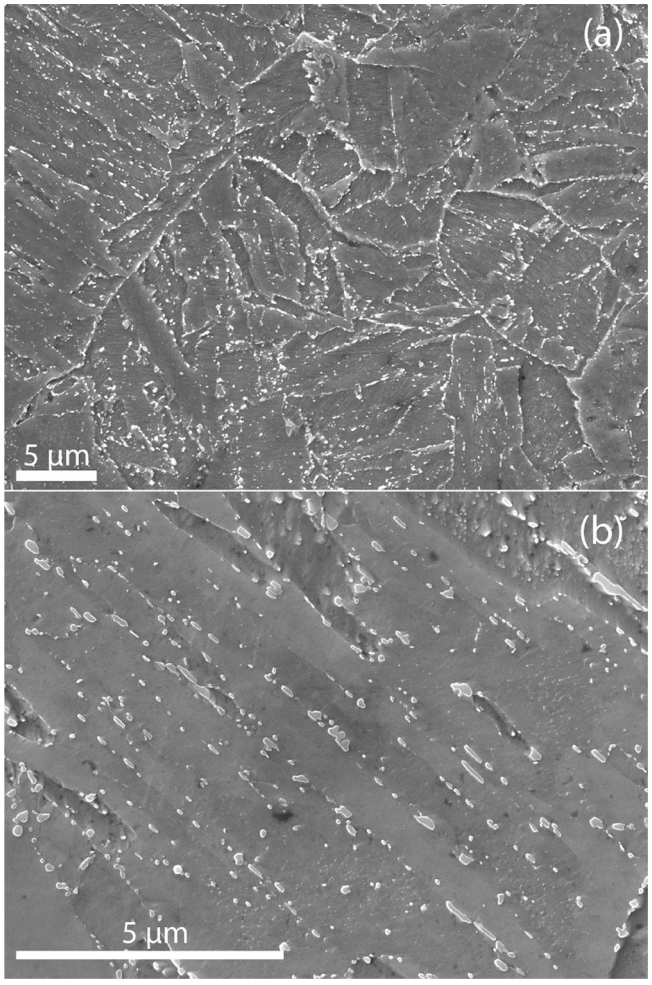

Fig. 3. SEM micrographs for the as-received T91 (T91-AR) in (a) high and (b) higher magnification.

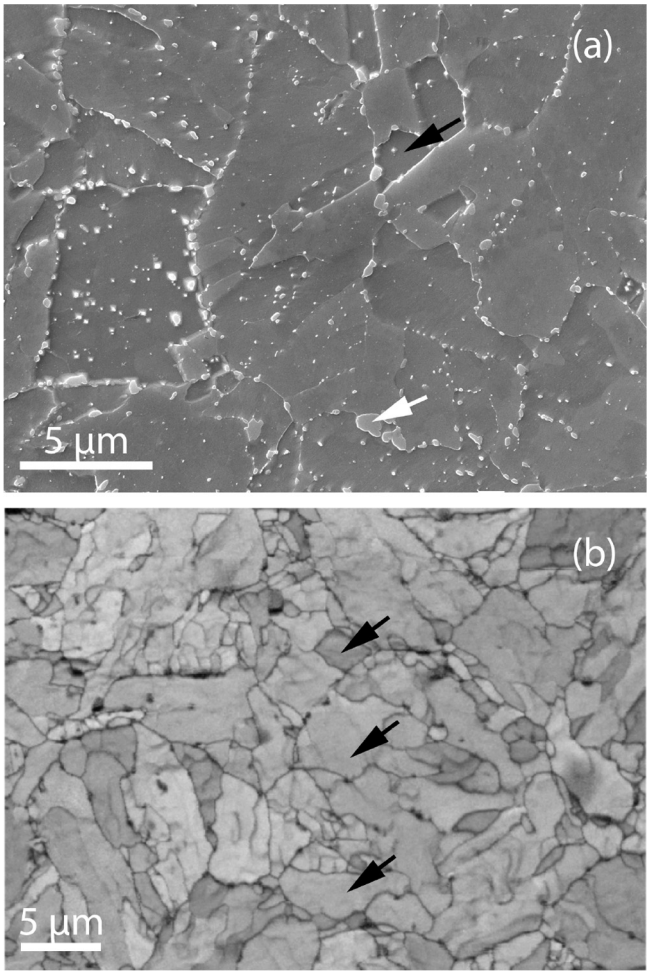

Fig. 5. Micrographs for the T91 as tempered at 780 °C for 100 h (T91-T100h) (a) SEM (b) EBSD image quality map. Examples of equi-axed subgrains and significantly coarsened carbide precipitates are marked by black and white arrows respectively.

different conditions using the cylindrical EM sensor. The real inductance is essentially independent of frequency over the low frequency (approximately 10–100 Hz) range then drops continuously with increasing frequency until it approaches a small negative value at very high frequencies (over approximately 0.1 MHz). For conciseness, the inductance value at low frequencies (here taken as the value for 10 Hz) has been used as a characteristic inductance parameter M_0 (as this is known to be sensitive to the relative permeability, μ_r, of the material); the values of which are given in Table 2.

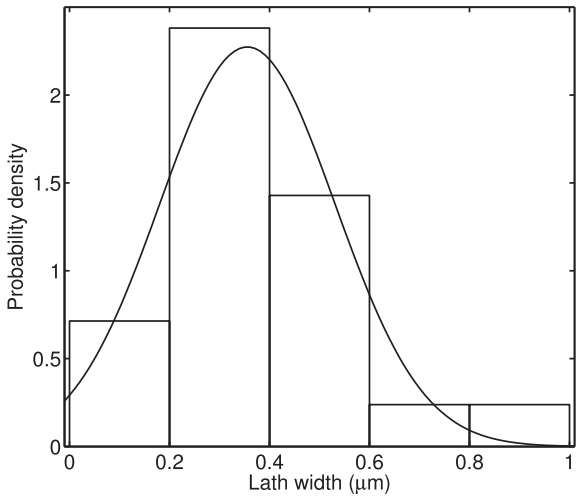

Fig. 4. Lath width distribution for the as received T91 (T91-AR) sample.

A 2D axisymmetric finite element (FE) model was developed for modeling the sensor signal output in response to a steel sample of given resistivity and relative permeability using Comsol Multiphysics software. The resistivity values of the modeled samples were taken from the experimental measurements and the relative permeability values determined by fitting the modeled real inductance with the experimental measurement based on a nonlinear least square method with 26 frequency points from 10 Hz to 1 MHz (logarithmically spaced) in Comsol LiveLink for Matlab. Close fits between the modeled and measured real inductance for all the samples have been achieved as shown in Fig. 8. It should be noted the EM measurement for the T91-ES sample is not directly comparable with the other samples because the sample length (50 mm – maximum possible from the component received) is only half the length of the other samples. However, the relative permeability, as a material property, is independent of sample geometry. The expected EM sensor response for a 100 mm length T91-ES sample was predicted with Comsol using the fitted relative permeability value and the measured resistivity value and is also shown on Fig. 8.

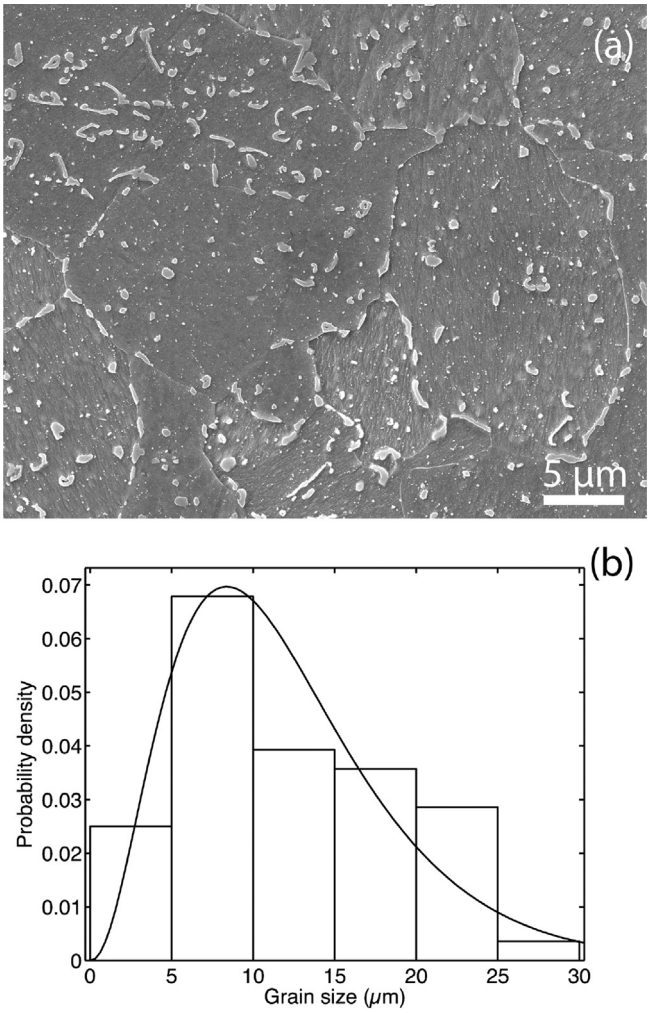

Fig. 6. (a) SEM micrograph and (b) grain size distribution for the mis-heat-treated T91 (T91-M) sample.

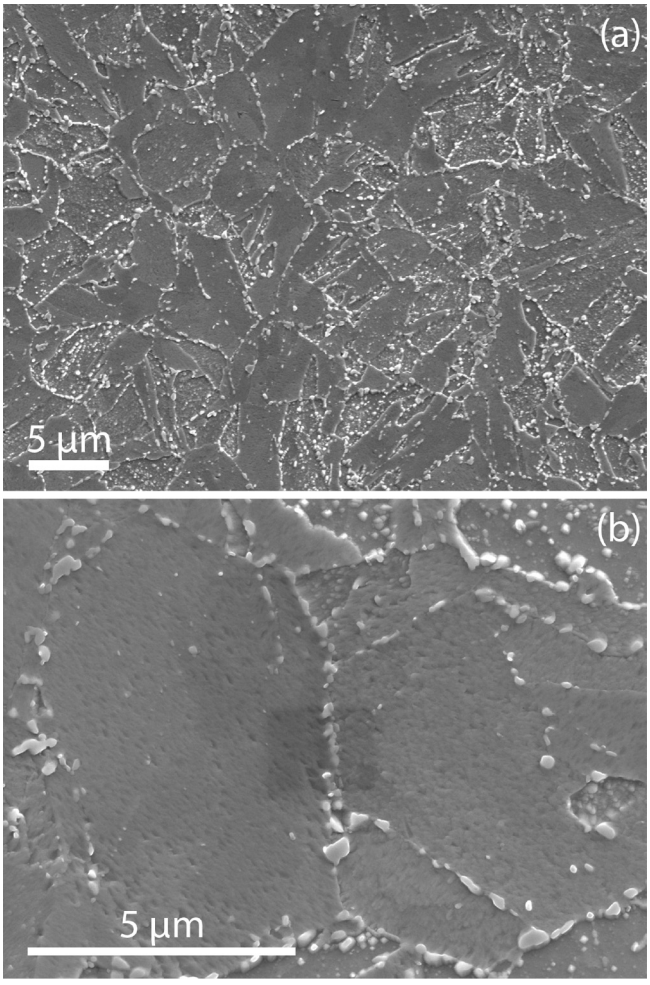

Fig. 7. SEM micrographs for the ex-service T91 tubes (T91-ES) at (a) high and (b) higher magnification.

It can be seen from Fig. 8 and Table 2 that the T91 samples in the different conditions can be clearly distinguished from each other, from the inductance parameter M_0, using the cylindrical EM sensor.

It should be noted that the present laboratory-based EM sensor are sensitive to initial permeability or relative permeability for small magnetic fields, where domain wall motion can be treated as approximately reversible. That is, domain walls return to their original positions after application and removal of an applied field or, in an alternated current field, oscillate between neighboring pinning sites. This has been discussed in our previous paper [16], which demonstrated that the low frequency inductance, M_0, increase with the initial relative permeability exponentially and the latter is affected by the microstructural features that determine the mean free path for domain wall motion in a small magnetic field. For the service-entry T91 (T91-AR) samples martensitic lath boundaries are the predominant pinning features to domain wall motion. The precipitates on the lath/grain boundaries play a minor role in pinning domain wall motion. Therefore the mean free path to domain wall motion is determined by the martensitic lath width. For the mis-heat treated sample (T91-M) both the precipitates within the grains and the grain boundaries are major pinning sites to domain wall motion whilst the precipitates on the grain boundaries play a minor role in domain wall motion. In this case, the mean free path is determined by the mean spacing between the pinning features (i.e. the intra-grain particles and the grain boundaries) or, equivalently, by the number density of the precipitates and the grain boundaries (i.e. the grain size). The significantly higher relative permeability of the mis-heat treated samples

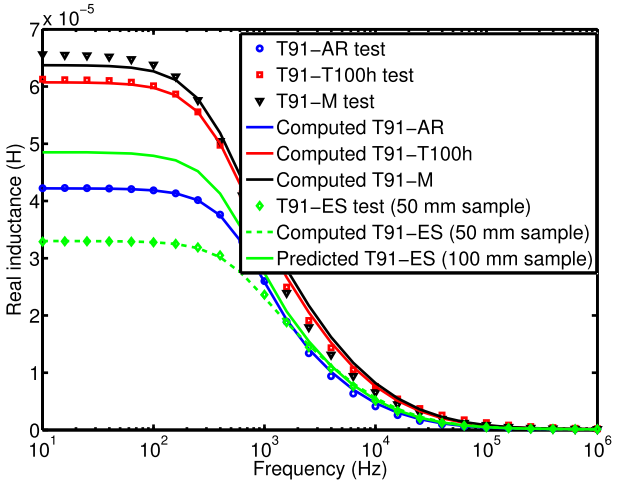

Fig. 8. Measured and computed real inductance as a function of frequency for the studied T91 samples in the different conditions (the suffixes AR, T100h, M and ES denote as received, as tempered at 780 °C for 100 h, mis-heat treated and ex-service respectively.).

Table 2
Measured Vickers hardness and EM values for the T91 samples in the different conditions.

Samples	Hardness (HV)	Resistivity ($\times 10^{-7}\Omega\cdot m$)	M_0 ($\times 10^{-5}$ H)	μ_r[a]	H_c (kA/m)	H_c^* (kA/m)
T91-AR	237±2.1	5.112±0.019	4.224±0.014	92	1.01	1.11
T91-T100h	195±2.2	5.099±0.035	6.127±0.004	161	0.90	0.86
T91-M	157±3.5	5.085±0.043	6.563±0.008	177	0.70	0.57
T91-ES	219±3.4	4.810±0.036	4.850±0.008	112	–	–

[a] μ_r was not directly measured but obtained by fitting the modelled EM sensor signals with experimental measurements.

can therefore be attributed to the increased mean free path to domain wall motion due to the inter particle spacing (and grain size) being larger than the martensitic lath size of the T91-AR sample. For the as-tempered T91 (T91-T100h) and the ex-service T91 (T91-ES) samples two types of microstructural features, i.e. the lath boundaries and the sub-grain boundaries, are effective pinning features to domain wall motion. Therefore the mean free path to domain wall motion, and hence the relative permeability, are collectively determined by the martensitic lath widths and the sub-grain size. Accordingly, the significant coarsening of the martensitic laths as well as the sub-grain development after the accelerated long tempering increase the mean free path to domain wall motion and hence the relative permeability significantly. Similarly, the slightly greater relative permeability for the ex-service (T91-ES) than the as-received T91 (T91-AR) is expected of the coarsening of the martensitic laths and the sub-grain development increasing the mean free path to domain wall motion after the service exposure.

3.2.2. Laboratory-based major BH loop measurements

Fig. 9 shows the major BH loops for the T91 samples in the different conditions measured using the lab-based BH measurement system on the cylindrical samples. The three samples can be clearly distinguished. The measured coercivity, H_c, values (extracted from the BH loops) dropped by approximately 9% and 31% after the accelerated tempering and the mis-heat treatment respectively, as can be seen in Table 2. The trend in H_c values follows a qualitatively similar trend to the Vickers Hardness. The agreement in these trends indicates that as reported in the literature e.g. Ref. [7] there is a relationship between mechanical and magnetic hardness. The drop in the coercivity value after accelerated tempering can be attributed to lath coarsening, sub-grain development and further recovery of dislocations reducing the number density of microstructural features impeding domain wall motion. In addition, a smaller reverse field is required for the domain walls to overcome the pinning from these features and bring the sample with remanence (i.e. the remaining magnetic induction after the magnetic field has been removed) back to zero induction. The precipitates on the boundaries play a relatively minor role in pinning domain walls, as the boundaries are major pinning features in this case. The precipitates within the sub-grains become effective in pinning domain walls and tend to increase the coercivity. However, as the lath and sub-grain boundaries are predominant pinning features for the as-tempered T91 (T91-T100h), the net effect is an increase in the overall pinning to domain walls, and hence a decrease in coercivity. The lower coercivity value for the mis-heat-treated sample is expected as the ferritic structure is magnetically softer than a martensitic structure owing to its lower dislocation density and larger grain size compared to the lath width and sub-grain size (or equivalently lower number density of boundaries), which overweigh the magnetic hardening (i.e. increase in coercivity) effect of the large precipitates within the ferrite grains.

3.2.3. Major loop measurements on tube samples

Fig. 10 shows the *equivalent* major loops—with a same applied amplitude of excitation current as that for the cylindrical sample measurement—measured using the system shown in Fig. 2 on the T91 tube samples in the three different conditions. Generally the measured coercive force for the amplitude($\approx$ 3.4 kA/m) of the major loop for the tube samples, H_c^*, follow the same trend as the measurements on the machined cylindrical samples, as described in Table 2. It should be noted that, as illustrated in a magnetic flux density distribution map of the tube cross-section during a test as schematically shown in Fig. 2, the shape of the loops is different due to the particular arrangement of the B value measurement and non-uniform B and H field distributions in the tube samples. If the measurements using this system are to be comparable to those

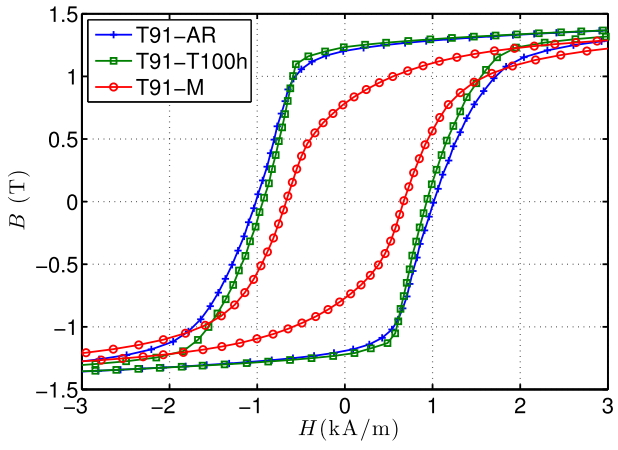

Fig. 9. Major BH loops for the T91 samples in the as received (T91-AR), as tempered (T91-T100h) or as mis-heat treated (T91-M) conditions measured using the laboratory-based BH measurement system on the cylindrical samples, for the [-3 3] kA/m region. The full amplitude of H for the measurements was approximately 36.4 kA/m to ensure saturation of the samples.

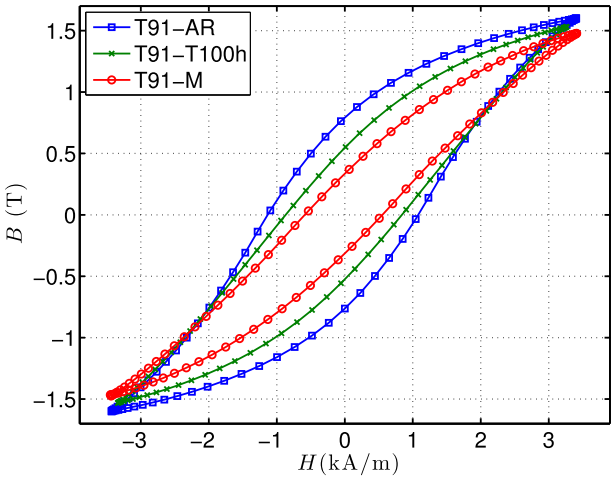

Fig. 10. Major BH loops for the T91 tube samples in the as received (T91-AR), as tempered (T91-T100h) or as mis-heat treated (T91-M) conditions.

from the cylindrical samples and comparable between measurements with different pipe diameters, some calibration of the B value must be carried out. However, it is clear from these results, on a single tube diameter, that the industrial deployable sensor for tube samples can be used to separate correctly heat treated and mis-heat treated microstructures at service entry, and can distinguish microstructural changes due to accelerated ageing.

4. Conclusions

The laboratory-based measurements using both the EM sensor systems and BH loop measurement system have proved capable of distinguishing all the heat-treated and the ex-service T91 samples from the service-entry one. Generally the measured coercivity values for the demonstration tube samples follow the same trend as the measurements on the machined cylindrical samples although there is a sample geometry effect on the absolute values of measured coercivity as well as the shape of the major loops. The results indicate that an industrial deployable sensor system can be used for sorting service-exposed or mis-heat-treated/mis-manufactured Grade 91 steel tubes/pipes from the correctly heat treated service-entry ones provided the tubes/pipes are of same diameter or geometry effect can be addressed with necessary calibration of the measured coercivity or other EM sensor signals.

Acknowledgement

This work was carried out with financial support from EPSRC (EP/H023429/1) and EPRI under the grant UOBKTS002. The authors would like to thank EPRI and Ken Mitchell at RWE npower for providing the steel tubes and David Allen at E.ON for providing the mis-heat treatment procedure and industrial furnaces for the heat treatments of the demonstration tube samples at E.ON.

References

[1] H.K.D.H. Bhadeshia, A. Strang, D.J. Gooch, Ferritic power plant steels: remanent life assessment and approach to equilibrium, Int. Mater. Rev. 43 (2) (1998) 45–69.
[2] EPRI, Service Experience with Grade 91 Components, 2009, 1018151.
[3] EPRI, Review of Weld Repair Options for Grade 91, Part 2: Damage Development and Distribution, 2013, 3002000087.
[4] J. Parker, In-service behavior of creep strength enhanced ferritic steels Grade 91 and Grade 92 –Part 1 parent metal, Int. J. Pressure Vessels Piping 101 (2013) 30–36.
[5] A. Mitra, J.N. Mohapatra, J. Swaminathan, M. Ghosh, A.K. Panda, R.N. Ghosh, Magnetic evaluation of creep in modified 9Cr-1Mo steel, Scr. Mater. 57 (9) (2007) 813–816.
[6] J.N. Mohapatra, J. Swaminathan, M.K. Ghosh, A. Mitra, Magnetic nondestructive evaluation of creep behavior in water-quenched modified 9Cr-1Mo steel, Metall. Mater. Trans. A 41 (4) (2010) 900–905.
[7] H. Kumar, J.N. Mohapatra, R.K. Roy, R. Justin Joseyphus, A. Mitra, Evaluation of tempering behaviour in modified 9Cr–1Mo steel by magnetic non-destructive techniques, J. Mater. Process. Technol. 210 (4) (2010) 669–674.
[8] V. Moorthy, S. Vaidyanathan, T. Jayakumar, B. Raj, On the influence of tempered microstructures on magnetic Barkhausen emission in ferritic steels, Philos. Mag. A 77 (6) (1998) 1499–1514.
[9] C.J. Bong, K.S. Ryu, S.H. Nahm, E.K. Kim, Nondestructive evaluation for remanent life of modified 9Cr-1Mo steel by reversible magnetic permeability, J. Magn. Magn. Mater. 323 (5) (2011) 379–382.
[10] W. Yin, X.J. Hao, A.J. Peyton, M. Strangwood, C.L. Davis, Measurement of permeability and ferrite/austenite phase fraction using a multi-frequency electromagnetic sensor, NDT&E Int. 42 (1) (2009) 64–68.
[11] S.J. Dickinson, R. Binns, W. Yin, C. Davis, A.J. Peyton, The Development of a multifrequency electromagnetic instrument for monitoring the phase transformation of hot strip steel, IEEE Trans. Instrum. Meas. 56 (3) (2007) 879–886.
[12] A. Peyton, C. Davis, P. Morris, F.D. Van Den Berg, P. Hunt, On line electromagnetic inspection of steel microstructure during hot processing, in: 1st European Steel Technology & Application Days & 31st Journées Sidérwrurgiques Internationales (JSI), 2014.
[13] X. Hao, W. Yin, M. Strangwood, A. Peyton, P. Morris, C. Davis, Characterization of decarburization of steels using a multifrequency electromagnetic sensor: experiment and modeling, Metall. Mater. Trans. A 40 (4) (2009) 745–756.
[14] X.J. Hao, W. Yin, M. Strangwood, A.J. Peyton, P.F. Morris, C.L. Davis, Off-line measurement of decarburization of steels using a multifrequency electromagnetic sensor, Scr. Mater. 58 (11) (2008) 1033–1036.
[15] R.J. Haldane, W. Yin, M. Strangwood, A.J. Peyton, C.L. Davis, Multi-frequency electromagnetic sensor measurement of ferrite/austenite phase fraction–Experiment and theory, Scr. Mater. 54 (10) (2006) 1761–1765.
[16] J. Liu, M. Strangwood, C. Davis, A. Peyton, Magnetic evaluation of microstructure changes in 9Cr-1Mo and 2.25Cr-1Mo steels using electromagnetic sensors, Metall. Mater. Trans. A 44 (13) (2013) 5897–5909.
[17] J. Liu, M. Strangwood, C.L. Davis, J. Parker, Non-destructive characterisation of N/Al level in P91 steels using electromagnetic sensors, Mater. Sci. Technol. 31 (9) (2015) 1042–1050.
[18] P.K. Heywood, Elevated Temperature Tensile Test and Microstructure/Hardness Examination of P91 Header Material: Results of tests on Materials 'As Supplied from the Mill' and after 'Anomalous Heat Treatment', TEi Metallurgical Service, 2006. MS201B/06.
[19] N. Haned, M. Missous, Nano-tesla magnetic field magnetometry using an InGaAs–AlGaAs–GaAs 2DEG Hall sensor, Sensors Actuators A Phys. 102 (3) (2003) 216–222.
[20] H. Ghassemi-Armaki, R.P. Chen, K. Maruyama, M. Yoshizawa, M. Igarashi, Static recovery of tempered lath martensite microstructures during long-term aging in 9–12% Cr heat resistant steels, Mater. Lett. 63 (28) (2009) 2423–2425.
[21] EPRI, Life Management of Creep Strength Enhanced Grade 91 Steel – Atlas of Microstructure, 2013, 3002000080.
[22] C.G. Panait, A. Zielinska-Lipiec, T. Koziel, A. Czyrska-Filemonowicz, A.F. Gourgues-Lorenzon, W. Bendick, Evolution of dislocation density, size of subgrains and MX–type precipitates in a P91 steel during creep and during thermal ageing at 600 °C for more than 100,000h, Mater. Sci. Eng. A 527 (16–17) (2010) 4062–4069.
[23] V. Thomas Paul, S. Saroja, M. Vijayalakshmi, Microstructural stability of modified 9Cr-1Mo steel during long term exposures at elevated temperatures, J. Nucl. Mater. 378 (3) (2008) 273–281.